Primary and Secondary Dimer Interfaces of the FGFR3 Transmembrane Domain: Characterization via Multiscale Molecular Dynamics Simulations

Tyler Reddy[1], **Santiago Manrique**[1,2], **Amanda Buyan**[1], **Benjamin A. Hall**[1,3], **Alan Chetwynd**[1], and **Mark S.P. Sansom**[1]

[1]Department of Biochemistry, University of Oxford, South Parks Road, Oxford, OX1 3QU, U.K.

[2]Division of Structural Biology, Wellcome Trust Centre for Human Genetics, University of Oxford, Oxford, OX3 7BN, U.K.

[3]Current address: Microsoft Research Cambridge, 21 Station Road, Cambridge, CB1 2FB, U.K.

Abstract

Receptor tyrosine kinases are single pass membrane proteins which form dimers within the membrane. The interactions of their transmembrane domains (TMDs) play a key role in dimerization and signaling. The fibroblast growth factor receptor 3 (FGFR3) is of interest as a G380R mutation in its TMD is the underlying cause of ~99% of cases of achondroplasia, the most common form of human dwarfism. The structural consequences of this mutation remain uncertain: the mutation shifts the position relative of the TMD relative to the lipid bilayer but does not alter the association free energy. We have combined coarse-grained and all-atom molecular dynamics simulations to study the dimerization of wild-type, heterodimer, and mutant FGFR3 TMDs. The simulations reveal that the helices pack together in the dimer to form a flexible interface. The primary packing mode is mediated by a Gx_3G motif. There is also a secondary dimer interface which is more highly populated in heterodimer and mutant configurations which may feature in the molecular mechanism of pathology. Both coarse-grained and atomistic simulations reveal a significant shift of the G380R mutant dimer TMD relative to the bilayer so as to enable interactions of the arginine sidechain with lipid head group phosphates.

Introduction

Receptor tyrosine kinases (RTKs) are single pass membrane proteins. They have a extracellular ligand-binding ectodomain, a α-helical single transmembrane domain (TMD), and an intracellular kinase domain (1). They form dimers within the membrane, and a number of NMR structures of TMD dimers in membrane-like environments have been determined (2–8). However, in the absence of a high resolution structure for an intact RTK, important aspects of the conformational dynamics of the TMD dimers in relation to signaling remain unknown.

*To whom communications should be addressed: mark.sansom@bioch.ox.ac.uk phone: +44 1865 613306.

Many RTKs are important in the context of human disease. The fibroblast growth factor receptor 3 (FGFR3) is of particular interest as a G380R mutation in its TMD is the underlying cause of ~99% of cases of achondroplasia, the most common form of human dwarfism (9). Although the genetic basis for achondroplasia has been known for nearly two decades the molecular mechanism of pathology remains uncertain. FGFR3 is a negative regulator of bone growth and there is experimental evidence for increased signaling by the mutant receptor (10). It is thus of interest to understand the effects of the G380R mutation on the behavior of the TMD dimer at a fundamental biophysical level.

The free energies of dimerization, as measured by FRET in a POPC lipid bilayer for wild-type and G380R TMD peptides, match one another within the bounds of experimental uncertainty (11) indicating that perturbation of dimerization propensity *per se* is unlikely to be the key effect of this particular mutation. Significantly, neutron diffraction and oriented circular dichroism indicate a 5 Å 'vertical' shift of the G380R mutant peptide relative to the centre of a lipid bilayer (12). Thus there is an apparent conceptual disconnect between the significant shift in position relative to the lipid bilayer and the unperturbed association free energy of the mutant FGFR3 TMD, which merits further investigation. Importantly, recent experimental evidence indicates that a different pathogenic mutation of FGFR3, A391E, leads to an increase in dimer stability (-1.5 kcal/mol) independent of whether the FGFR3 TMDs are studied in isolation or with their large ectodomains attached (13). This supports the validity of studying the interactions of FGFR3 TMDs in isolation in order to better understand the conformational dynamics of the more complex intact receptor. It also indicates that some mutations may act via changing dimer stability whilst other mutations may perturb TMD dimers in a different fashion.

There have been a number of NMR studies of TMD dimers from a range of RTKs including e.g. the ErbB receptors (2–5) and the EphA receptors (6, 7). These have revealed a variety of packing modes and motifs. Furthermore, a combination of experimental (14, 15) and computational (1, 16) approaches have recently emphasized the importance of the multiple modes of interaction of TMDs within dimers as playing a key role in signaling by RTKs (17). A recent NMR structure of the FRFR3 TMD dimer (8) in a detergent (DPC/SDS) micelle environment, which reveals a helix packing mode dominated by an extended hydrophobic heptad, has been interpreted in the context of mapping of the location of pathogenic mutations as suggesting a putative alternative helix interface which is formed upon receptor activation.

Molecular dynamics (MD) and related simulations are able to provide insights into TMD dimerization, both of model systems such as glycophorin (GpA e.g. (18–21)), and of RTKs, especially ErbBs (e.g. (14, 16, 22, 23)). To date, relatively short time scale (50 ns) atomistic simulations have been performed on FGFR3 TMDs, with selection of starting configurations from a Monte Carlo search in a simplified implicit bilayer model (24), suggesting multiple packing modes for the TMD helices within the dimer.

Here we study the dimerization of FGFR3 TMD constructs over extended (μs) time scales using coarse-grained (CG) MD simulations (25). This approach has been previously used to successfully model GpA (26) TMD dimerization, providing results consistent with high-

resolution experimental structures and mutagenesis results. Representative TMD dimers formed in these CG simulations are refined by atomistic (AT) MD simulations, providing a multiscale approach to FGFR3 TMDs, as used in e.g. previous studies of integrin TMD dimers (27). We focus on the G380R mutation and compare FGFR3 wild-type, heterodimer, and mutant homodimer TMDs in terms of both helix-helix and protein-lipid interactions. Significantly, our simulations of the wild-type TMD reveal a predominant packing mode which corresponds to the activated state proposed by Bocharov et al. (8).

Materials and Methods

CG Simulations

Coarse-grained simulations (Table 1) were performed in GROMACS 4.0.x (28) using a previously described (25) local version of the MARTINI forcefield (29–31), which employs an approximate 4:1 mapping of heavy atoms to representative particles. The CG simulations were conducted at 323 K with separate temperature coupling for protein, lipid and solvent using the Berendsen thermostat (32). Timesteps of 40 fs duration were used with frames written every 400 ps. Coulomb and VDW interactions were shifted to 0 between 0-12 Å and 9-12 Å, respectively. Semi-isotropic pressure coupling was performed using the Berendsen algorithm with a 1.0 ps time constant, 5×10^{-6} bar^{-1} compressibility, and 1.0 bar reference pressure. Replicate simulations employed different starting velocity seeds. Final simulation box sizes varied slightly, with approximate dimensions 10.5 nm $\times$ 10.5 nm$\times$11.5 nm. WT, WT/G380R heterodimer, and G380R homodimer systems had slightly different compositions with approximately 330 POPC molecules, 6400 water molecules, and a small number of neutralizing Cl$^-$ ions.

The TMDs were modeled as ideal α-helices. The initial separation between the TMD helices in the CG simulations was ~55 Å (see Figure 1A), the same value used in previous GpA CG simulations (26), and outside the 12 Å long-range interaction cutoff for this forcefield. The initial systems with separated helices were generated by 200 ns simulations, in which POPC bilayers were self-assembled around position-restrained protein TMDs, as described previously (33).

Atomistic Simulations

Initial AT simulation systems were generated from representative CG TMD dimer structures using our CG2AT protocol as described previously (34). Representative average structures were obtained using the g_cluster module of GROMACS. The resulting AT system was energy minimized and equilibrated (duration 1 ns) with a position restraint on protein Ca atoms (force constant = 10 kJ/mol/Å). Unrestrained simulations were performed with a time step of 2 fs and a total duration of 100 ns per simulation. Semi-isotropic pressure of 1 bar was applied using a Parinello-Rahman barostat (35) and the temperature was maintained at 323 K with a Berendsen thermostat (32). Electrostatic interactions were modeled using a particle-mesh Ewald summation (cutoff distance 10 Å, also used for van der Waals interactions). The bond lengths were restricted using the LINCS algorithm (36). GROMACS 4.5.4 (28) was used in combination with the GROMOS96 43a forcefield (37).

Trajectory analysis and visualization

CG-MD trajectories were exposed using the MDAnalysis library (38), and parsed using in-house Python code detailed in the algorithm descriptions provide in the Supporting Information. AT-MD trajectories were analyzed using the GROMACS 4.5.4 (27) tools. Visualization was performed with VMD (39).

Results and Discussion

TMD Dimerization

We performed ensembles of 5 μs duration dimerization simulations for wildtype (WT) and mutant (see Table 1) FGFR3 TMD helices and for (control) GpA TMDs, with the two TMD monomers initially separated by ~55 Å in POPC bilayers (Figure 1). As previously seen for GpA (26), there was stochastic variation in the time required for initial dimer formation (SI Figure S1), corresponding to the use of random initial velocities (consistent with a Maxwellian distribution at the stated temperature) for each simulation within an ensemble. There did not seem to be any substantial difference in the time to dimer formation between the FGFR3 WT, WT/G380R, and G380R simulations, although much larger ensembles (typically of 100 or more simulations) would be needed to more accurately explore any differences in dimerization times. In many simulations one helix wanders substantially within the bilayer plane before dimer formation relative to the other helix (Figure 1C). Thus the stochastic dimerization times and substantial translational (and rotational) motions of the helices relative to one another within the bilayer plane are consistent with a simulation protocol that is not biased towards formation of a particular dimer interface. Both the GpA and the FGFR3 TMDs formed stable dimers in our CG simulations, with no observations of subsequent dissociation of the helices. Indeed, atomistic (14) simulations of the related EGFR TMDs indicate that extended (>10 μs) simulations are likely to be needed to observe TMD dimer dissociation events. We examined the bilayer thickness around the TMDs (SI Figure S2) and although a small degree of thinning (1 to 2 Å) was observed adjacent to the FGFR3 TMDs this was the same before and after dimerization, suggesting that the bilayer thickness is unlikely to have a major effect on dimerization.

Having confirmed the formation of stable dimers in an unbiased fashion in our simulations, we have analyzed the properties of the dimer configurations in detail. Our control GpA TMD dimers in POPC bilayers consistently exhibited right-handed helix crossing angles (Figure 2A), as previously reported for GpA simulations in DPPC (19, 20, 26), and consistent with experimental NMR structures of the GpA TMD (40, 41). In contrast, the FGFR3 TMD helices did not show a strong preference for a left-or right-handed helix packing, instead exhibiting bimodal distributions of crossing angles. There is a slight preference for left-handed helix packing for wild-type FGFR3 relative to WT/G380R heterodimer and G380R mutant homodimers. The bimodal distribution may result from FGFR3 helices adopting different crossing angles as they oscillate closer or farther apart in the dimer, although the helix crossing angles appear to be largely independent of the closest approach distance of the helices (Figure 2B), with a bimodal distribution at a single optimal distance. The FGFR3 helices thus form stable dimers but exhibit a broad range of helix crossing angles suggestive of a 'looser' interface than in e.g. GpA. To probe their relative

motions in the bilayer, the correlation coefficients for the z coordinates of the geometric centers of each helix were calculated before and after dimer formation (SI Figure S3). As expected, helix displacement motions were not correlated before dimer formation, but were strongly correlated after a dimer was formed. Significantly, GpA exhibits a more strongly correlated dimer motion (R = ~0.8) than all of the FGFR3 TMD dimers R = ~0.6). This is consistent with e.g. TOXCAT studies (42) suggesting the GpA TMD dimer is more stable than that of FGFR3. Given the somewhat weaker correlation of translation motion of FGFR3 helices within the dimer and the bimodal helix crossing angle distribution, we decided to examine the nature of the helix dimer interface more closely.

To identify the predominant residues within a (dynamic) interface, we calculated the normalized probability for each residue C_{α} on either helix to be in the top five closest interhelix contacts over the whole ensemble of simulations. To test this approach, the analysis was first performed on the GpA simulations. G79, G83, and T87 were identified as predominant contacts (SI Figure S4). Since these three residues have previously been identified as experimentally crucial interfacial contacts (see e.g. (43)), this analytical approach may confidently be applied to predict interfacial residues in the FGFR3 TMD.

Residues G370, A374, S378 and G382 (which form three consecutive small-x_3-small motifs) and also R397 stand out as important contacts from FGFR3 wild-type, heterodimer, and mutant homodimer simulations (Figures 3 and 4A), and other candidates are spaced at 3-4 residue intervals, consistent with identification of a helical interface. It is noteworthy that residues 380 and 391, involved in achondroplasia and Crouzon syndrome respectively (44), do not feature prominently in the closest contacts in FGFR3 dimer configurations. This is consistent with the lack of effect of the G380R mutation on dimerization propensity (11). G370, which is prominent in the closest contacts, is mutated to Cys in type 1 thanatophoric dysplasia, which is much more severe than achondroplasia and normally neonatal lethal (45). Thus, phenotype severity may, at least in part, reflect the proximity of the point mutation to the dimer interface. Furthermore, G370 was recently identified at the dimer interface by site specific infrared dichroism (46), and the propensity for disulfide formation in FGFR3 follows the trend C370 > C371 > C375 (47). Interestingly, R397, which is one of the top three major FGFR3 contacts we identify, is part of the CRLR C-terminal tetrapeptide which, if removed, increases the dimerization propensity of FGFR3 to match that of GpA (46).

Alternative Dimer Interfaces

The biological and experimental correlations with our candidate FGFR3 dimer interface residues are encouraging. However, the identification of a small set of major dimer contact residues does not explain how FGFR3 dimers can exhibit both left-and right-handed helix crossing angles. To explore the possibility of alternative dimer interfaces, one helix in each simulation was fixed to a reference structure and positional probability of the second helix in this reference frame determined (Figure 3). This analysis reveals a primary dimer interface for FGFR3 WT, heterodimer, and mutant TMDs. Importantly, a secondary dimer interface progressively begins to appear for the heterodimer and is most pronounced in the mutant homodimer simulations. Interestingly, tracking dimer configuration in this fashion as a

function of simulation time revealed that there are discrete periods within a simulation when the dimer adopts one of the two interfaces along with a clear transition point from one interface to the other, rather than e.g. a continuous switching between the two interfaces (Figure 5). There is however considerably more motion about the secondary interface, which is consistent with a dimer configuration of lower stability.

Further analysis of the motion of helix 2 relative to the (fixed) helix 1 reveals a correlation of the polar angle (θ) defining the relative position of helix 2 within the bilayer plane with interhelix crossing angle (Ω; SI Figure S5). Thus the primary dimer interface (I1 in Fig. 3) exhibits a bimodal helix crossing angle about zero degrees while the secondary dimer interface (I2 in Fig. 3) observed in the FGFR3 heterodimer and mutant homodimer exhibits a predominantly right-handed helix crossing angle. Using the value of θ as a means to classify dimer interfaces across all FGFR3 trajectories, we repeated the dimer interface contact analysis for the classified trajectories and discovered a striking loss of interfacial symmetry at G370, which is a prominent contact for *both* helices at the primary interface but only for one at the secondary interface (Figure 4BC). The secondary dimer interface also loses symmetry at the important R397 contact.

The presence of a secondary dimer interface in FGFR3 mutant heterodimer and mutant homodimer configurations suggests that rearrangement of these TMDs may be a component of the molecular mechanism of pathology in achondroplasia. The rearrangement, a rotation of one helix relative to the other, may provide a gain of function to the attached intracellular kinase domains. Indeed, changes in helix packing within TMD dimers (48) have been suggested as possible activation mechanisms in e.g. recent combined experimental and computational studies of EGFR (1, 14) activation and on the basis of computational studies of FGFR3 dimers (24). Furthermore, the oncogenic V664E TMD mutation in Neu (i.e. the rat homologue of ErbB2) prevents conformational switching between the active and inactive states (49). Thus, the plasticity of the TMD helix dimer interfaces in RTKs seems likely to play a key role in conformational switching underlying receptor activation.

The G380R Mutation and Bilayer Interactions

Our results indicate that the G380R mutation promotes adoption of a secondary interface, even though this residue is located opposite interfacial residues. Furthermore, experimental studies have indicated that the G380R mutation leads to a translation of the TMD along the bilayer normal (12). To further explore the structural and functional implications of this mutation we have examined the protein-lipid interactions and the positions of WT and mutant TMD dimers relative to the bilayer. Calculation of the average TMD dimer position relative to the bilayer normal (z-position) suggests that in the CG simulation the G380R mutant induces a translation of ~4 Å along the bilayer normal towards the upper (i.e. extracellular) membrane leaflet. Clustering of structures from a second CG simulation ensemble with shorter durations but higher repeat number (see Table 1) yielded representative structures for the primary interface (I1) TMDs of WT and G380R FGFR3 (Figure 6AB). The representative structure for the FGFR3 G380R dimer (Fig. 6B) shows that both of the R380 sidechains are directed towards the upper membrane leaflet where they are able to interact with the negatively charged phosphates of the lipid head groups. These

representative CG structures were converted to the corresponding atomistic models (34) in order to run short (0.1 μs) atomistic simulations (see Table 1). The final frame of the atomistic WT simulation represents a stable dimer, fully integrated into the lipid bilayer (Figure 6C). The primary dimer interface (I1) observed in the CG simulations is maintained. The final snapshot of the G380R mutant homodimer clearly shows the vertical translation of both Arg380 residues (Figure 6D), such that these sidechains interact with the phosphate headgroups of the upper leaflet. This 'snorkelling' effect of basic amino-acid sidechains in the hydrophobic membrane environment has been widely discussed in terms of stabilizing TMD localization within bilayers (see e.g. (50)) and also has been suggested to regulate signaling across the membrane by integrins (51). Comparing the movements of WT and G380R dimers relative to the membrane normal reveals an approximate difference in z position of ca. 5.5 Å (SI Figure S6), i.e. just a little more than in the CG simulations, and consistent with the different resolutions of the two methods. This agrees well with the displacement of the TMD in the mutant by 5 Å revealed by neutron diffraction studies (12). The TMD helices also tilt relative to the bilayer in the AT-MD simulations, such that helix tilt angle for WT simulation reached an average of ~33°whereas the tilt of the corresponding G380R simulation reached an average of ~42°. However, more extended AT simulations may be needed to obtain reliable estimates of tilt angle distributions (52).

In the WT TMD dimer both of the R397 residues are located close to the lipid headgroup phosphates of the lower (inner) leaflet (Figure 6E). This enables the two R397 residues of adjacent helices to remain close to one another. This interaction is in agreement with our CG-simulations, suggesting that R397 plays an important role in (lipid mediated) TMD dimer formation (Figure 4A). Furthermore, our AT-simulations confirm that both R399 residues reside in the cytoplasm and that both C396 residues are not involved in the dimer interface (Fig 6E).

Interestingly, concomitantly with the 5.5 Å translation induced by the G380R mutant, the C-terminal residues (i.e. $C_{396}RLR_{399}$) are pulled towards the core of the bilayer (Figure 6F). Consequently, the R399 sidechains occupy energetically favorable positions at the membrane-water interface which are occupied by the R397 residues in the WT TMD dimer. Intriguingly, the R397 residues are moved closer towards the membrane center (resulting in some degree of local thinning of the bilayer) which forces them to adopt a more 'snorkelling' conformation in order to retain the interaction of the guanidinium group with the lipid phosphates. This destabilizes the intermolecular R397/R397 interaction, resulting in more asymmetric rearrangement of the C-terminal region in which the C396 residues now form the main TMD dimer interaction. These findings support the suggestion derived from experimental data, that conformational changes at the CRLR tetrapeptide may serve as a conformational switch between different sates of activation/inactivation of the kinase (46).

Conclusions

Overall, our results reveal the presence of multiple possible FGFR3 TMD dimer interfaces, with their relative propensities influenced by the presence of point mutations. In the case of the G380R mutation, interactions of the arginine sidechain with lipid bilayer phosphates may play a role in shifting propensities. Interestingly, our observation of an asymmetric

secondary interface was also reported for the G380R FGFR3 TMD on the basis of combined Monte Carlo / atomistic MD simulations (24).

It is important to consider possible methodological limitations. It is recognized that CG simulations provide an approximation to more detailed, all atom treatments of helix/helix interfaces. However, recent studies suggest that the combined use of CG and subsequent atomistic simulations can accurately reproduce e.g. the NMR structure of the integrin TMD heterodimer (27). In part this is because multiple CG simulations allow exploration of a greater range of conformational and helix-packing space than would equivalent AT simulations on their own. Furthermore, comparison of atomistic (18) and CG (19, 20) simulations of glycophorin A dimerization suggest that the two methods yield comparable free energy profiles for the dimerization process. A further limitation is the use of a single simple phospholipid species in our simulations. Studies on e.g. GPCRs have shown how lipid composition may influence receptor association and function (53) and this is likely to also be of importance for the TMDs of receptor tyrosine kinases (23). Thus in future studies it will be important to include consideration of the multiple lipid species present in cell membranes, and their likely interactions with both the transmembrane and juxta-membrane domains of the FGFR3. However, it is likely that a full consideration of such lipid interactions and their influence on TMD dimerization will require more detailed characterization and comparison of energy landscapes of helix dimerization (22) which in turn is likely to require the use of enhanced sampling protocols (see e.g. (54)), even when using CG simulations.

One aspect which may benefit from future investigations is that of the kinetics of TMD association and dissociation. Recent atomistic (14) simulations of EGFR TMDs show that simulations longer than 10 μs are needed to observe TMD dimer dissociation events. Experimental observations of e.g. dimerization of a model TMD peptide (55) or refolding of bacteriorhodopsin (56) suggest timescales in excess of 1 sec. Clearly a complete characterization of the mechanism of TMD association and dissociation by simulations will require enhanced sampling procedures e.g. metadynamics (57).

It is informative to compare our model of the FGFR3 TMD dimer with the structure revealed by NMR studies of the dimer in detergent (DPC/SDS) micelles (8). In the NMR studies a different interface, involving an extended hydrophobic heptad motif, is seen. However, in relating the NMR structure to pathogenic mutations, the authors of the NMR study (8) suggest the existence of an alternative packing mode involving a Gx_3G (or rather a small-x_3-small) sequence motif formed by residues G370-x_3-A374-x_3-S378-x_3-G382. This is the motif seen in our primary interface (Fig. 4B) for the WT TMD. Thus comparison of the NMR and the current simulation studies reinforces the suggestion that the FGFR3 TMDs may be able to adopt different packing modes, with changes in environment (e.g. bilayer vs. micelle) or in interactions with the ectodomains (within the intact receptor) able to drive switching between them. In particular, it seems likely that the primary packing mode mediated by a Gx_3G motif may correspond to an activated state of the receptor both in terms of the effects of some pathogenic mutations located at this interface, and by comparison with the proposed activated state structure of the EGFR TMD dimer, as discussed in more detail in (8).

The presence of multiple interaction modes of TMDs is an emergent theme for a number of RTKs, and is likely to reflect the looser interactions between these helices than within the canonical tight binding interface of the GpA TMD dimer. This is likely to be of functional importance, allowing a RTK TMD dimer to form a 'multi-state switch' which can be regulated by extracellular and intracellular interactions of the intact receptor. In particular, it seems that interactions of the intramembrane and juxtamembrane (JM) domains, with one another (14) and with lipids (15), are likely to modulate the intrinsic TMD interactions. Our atomistic simulations indicate that the G380R mutation induces a movement of the receptor dimer towards the outer membrane leaflet resulting in a rearrangement of the C-terminal CRLR residues. Whether this effect plays a role in the mechanism of pathogenesis of achondroplasia by triggering larger scale structural changes of the JM domains may be probed in future simulation studies (58). Furthermore, the G380R mutation has been observed to cause a delay in FGFR3 down-regulation (59), possibly caused by altered interactions of the JM domain with intracellular components of this process (60).

Supplementary Material

Refer to Web version on PubMed Central for supplementary material.

Acknowledgments

References

1. Arkhipov A, Shan Y, Das R, Endres NF, Eastwood MP, Wemmer DE, Kuriyan J, Shaw DE. Architecture and membrane interactions of the EGF receptor. Cell. 2013; 152:557–569. [PubMed: 23374350]

2. Mineev KS, Bocharov EV, Arseniev AS. Spatial structure of the dimeric transmembrane domain of the growth factor receptor ErbB2 presumably corresponding to the receptor active state. JBiolChem. 2008; 283:6950–6956.

3. Mineev KS, Bocharov EV, Pustovalova YE, Bocharova OV, Chupin VV, Arseniev AS. Spatial structure of the transmembrane domain heterodimer of ErbB1 and ErbB2 receptor tyrosine kinases. J Mol Biol. 2010; 400:231–243. [PubMed: 20471394]

4. Mineev KS, Khabibullina NF, Lyukmanova EN, Dolgikh DA, Kirpichnikov MP, Arseniev AS. Spatial structure and dimer-monomer equilibrium of the ErbB3 transmembrane domain in DPC micelles. Biochim Biophys Acta Biomemb. 2011; 1808:2081–2088.

5. Bocharov EV, Mineev KS, Goncharuk MV, Arseniev AS. Structural and thermodynamic insight into the process of "weak" dimerization of the ErbB4 transmembrane domain by solution NMR. Biochim Biophys Acta Biomemb. 2012; 1818:2158–2170.

6. Bocharov EV, Mayzel ML, Volynsky PE, Goncharuk MV, Ermolyuk YS, Schulga AA, Artemenko EO, Efremov RG, Arseniev AS. Spatial structure and pH-dependent conformational diversity of dimeric transmembrane domain of the receptor tyrosine kinase EphA1. J Biol Chem. 2008; 283:29385–29395. [PubMed: 18728013]

7. Bocharov EV, Mayzel ML, Volynsky PE, Mineev KS, Tkach EN, Ermolyuk YS, Schulga AA, Efremov RG, Arseniev AS. Left-handed dimer of EphA2 transmembrane domain: helix packing diversity among receptor tyrosine kinases. Biophys J. 2010; 98:881–889. [PubMed: 20197042]

8. Bocharov EV, Lesovoy DM, Goncharuk SA, Goncharuk MV, Hristova K, Arseniev AS. Structure of FGFR3 transmembrane domain dimer: implications for signaling and human pathologies. Structure. 2013; 21:2087–2093. [PubMed: 24120763]

9. Bellus GA, Hefferon TW, Deluna RIO, Hecht JT, Horton WA, Machado M, Kaitila I, McIntosh I, Francomano CA. Achondroplasia is defined by recurrent G380R mutations of FGFR3. Amer J Human Genet. 1995; 56:368–373. [PubMed: 7847369]

10. Webster MK, Donoghue DJ. Constitutive activation of fibroblast growth factor receptor 3 by the transmembrane domain point mutation found in achondroplasia. EMBO J. 1996; 15:520–527. [PubMed: 8599935]

11. You M, Li E, Hristova K. The achondroplasia mutation does not alter the dimerization energetics of the fibroblast growth factor receptor 3 transmembrane domain. Biochem. 2006; 45:5551–5556. [PubMed: 16634636]

12. Han X, Mihailescu M, Hristova K. Neutron diffraction studies of fluid bilayers with transmembrane proteins: Structural consequences of the achondroplasia mutation. Biophys J. 2006; 91:3736–3747. [PubMed: 16950849]

13. Sarabipour S, Hristova K. FGFR3 transmembrane domain interactions persist in the presence of its extracellular domain. Biophys J. 2013; 105:165–171. [PubMed: 23823235]

14. Endres NF, Das R, Smith AW, Arkhipov A, Kovacs E, Huang YJ, Pelton JG, Shan YB, Shaw DE, Wemmer DE, Groves JT, et al. Conformational coupling across the plasma membrane in activation of the EGF receptor. Cell. 2013; 152:543–556. [PubMed: 23374349]

15. Matsushita C, Tamagaki H, Miyazawa Y, Aimoto S, Smith SO, Sato T. Transmembrane helix orientation influences membrane binding of the intracellular juxtamembrane domain in Neu receptor peptides. Proc Natl Acad Sci USA. 2013; 110:1646–1651. [PubMed: 23319611]

16. Zhang LQ, Sodt AJ, Venable RM, Pastor RW, Buck M. Prediction, refinement, and persistency of transmembrane helix dimers in lipid bilayers using implicit and explicit solvent/lipid representations: Microsecond molecular dynamics simulations of ErbB1/B2 and EphA1. Proteins: Struct Func Bioinf. 2013; 81:365–376.

17. Polyansky AA, Volynsky PE, Efremov RG. Multistate organization of transmembrane helical protein dimers governed by the host membrane. J Amer Chem Soc. 2012; 134:14390–14400. [PubMed: 22889089]

18. Hénin J, Pohorille A, Chipot C. Insights into the recognition and association of transmembrane α-helices. The free energy of α-helix dimerization in glycophorin A. J Amer Chem Soc. 2005; 127:8478–8484. [PubMed: 15941282]

19. Janosi L, Prakash A, Doxastakis M. Lipid-modulated sequence-specific association of glycophorin A in membranes. Biophys J. 2010; 99:284–292. [PubMed: 20655857]

20. Sengupta D, Marrink SJ. Lipid-mediated interactions tune the association of glycophorin A helix and its disruptive mutants in membranes. Phys Chem Chem Phys. 2010; 12:12987–12996. [PubMed: 20733990]

21. Psachoulia E, Marshall D, Sansom MSP. Molecular dynamics simulations of the dimerization of transmembrane α-helices. Acc Chem Res. 2010; 43:388–396. [PubMed: 20017540]

22. Prakash A, Janosi L, Doxastakis M. Self-association of models of transmembrane domains of ErbB receptors in a lipid bilayer. Biophys J. 2010; 99:3657–3665. [PubMed: 21112290]

23. Prakash A, Janosi L, Doxastakis M. GxxxG motifs, phenylalanine, and cholesterol guide the self-association of transmembrane domains of ErbB2 receptors. Biophys J. 2011; 101:1949–1958. [PubMed: 22004749]

24. Volynsky PE, Polyansky AA, Fakhrutdinova GN, Bocharov E, Efremov RG. Role of dimerization efficiency of transmembrane domains in activation of fibroblast growth factor receptor 3. J Amer Chem Soc. 2013; 135:8105–8108. [PubMed: 23679838]

25. Bond PJ, Wee CL, Sansom MSP. Coarse-grained molecular dynamics simulations of the energetics of helix insertion into a lipid bilayer. Biochem. 2008; 47:11321–11331. [PubMed: 18831536]

26. Psachoulia E, Bond PJ, Fowler PW, Sansom MSP. Helix-helix interactions in membrane proteins: coarse grained simulations of glycophorin helix dimerization. Biochem. 2008; 47:10503–105012. [PubMed: 18783247]

27. Kalli A, H BA, Campbell ID, Sansom MSP. A helix heterodimer in a lipid bilayer: structure prediction of the structure of an integrin transmembrane domain via multiscale simulations. Structure. 2011; 19:1477–1484. [PubMed: 22000516]

28. Hess B, Kutzner C, van der Spoel D, Lindahl E. GROMACS 4: algorithms for highly efficient, load-balanced, and scalable molecular simulation. J Chem Theor Comp. 2008; 4:435–447.

29. Marrink SJ, de Vries AH, Mark AE. Coarse grained model for semiquantitative lipid simulations. J Phys Chem B. 2004; 108:750–760.

30. Marrink SJ, Risselada J, Yefimov S, Tieleman DP, de Vries AH. The MARTINI forcefield: coarse grained model for biomolecular simulations. J Phys Chem B. 2007; 111:7812–7824. [PubMed: 17569554]

31. Monticelli L, Kandasamy SK, Periole X, Larson RG, Tieleman DP, Marrink SJ. The MARTINI coarse grained force field: extension to proteins. J Chem Theor Comp. 2008; 4:819–834.

32. Berendsen HJC, Postma JPM, van Gunsteren WF, DiNola A, Haak JR. Molecular dynamics with coupling to an external bath. J Chem Phys. 1984; 81:3684–3690.

33. Reddy T, Rainey JK. Multifaceted substrate capture scheme of a rhomboid protease. J Phys Chem B. 2012; 116:8942–8954. [PubMed: 22770371]

34. Stansfeld PJ, Sansom MSP. From coarse-grained to atomistic: a serial multi-scale approach to membrane protein simulations. J Chem Theor Comp. 2011; 7:1157–1166.

35. Parrinello M, Rahman A. Polymorphic transitions in single-crystals - a new molecular-dynamics method. J Appl Phys. 1981; 52:7182–7190.

36. Hess B, Bekker H, Berendsen HJC, Fraaije JGEM. LINCS: A linear constraint solver for molecular simulations. J Comp Chem. 1997; 18:1463–1472.

37. Scott WRP, Hunenberger PH, Tironi IG, Mark AE, Billeter SR, Fennen J, Torda AE, Huber T, Kruger P, van Gunsteren WF. The GROMOS biomolecular simulation program package. J Phys Chem A. 1999; 103:3596–3607.

38. Michaud-Agrawal N, Denning EJ, Woolf TB, Beckstein O. MDAnalysis: a toolkit for the analysis of molecular dynamics simulations. J Comput Chem. 2011; 32:2319–2327. [PubMed: 21500218]

39. Humphrey W, Dalke A, Schulten K. VMD - Visual Molecular Dynamics. J Molec Graph. 1996; 14:33–38. [PubMed: 8744570]

40. MacKenzie KR, Prestegard JH, Engelman DM. A transmembrane helix dimer: structure and implications. Science. 1997; 276:131–133. [PubMed: 9082985]

41. Smith SO, Song D, Shekar S, Groesbeek M, Ziliox M, Aimoto S. Structure of the transmembrane dimer interface of glycophorin A in membrane bilayers. Biochem. 2001; 40:6553–6558. [PubMed: 11380249]

42. Finger C, Escher C, Schneider D. The single transmembrane domain of human tyrosine kinases encode self interactions. Science Signal. 2009; 2:ra56, 51–58.

43. Treutlein HR, Lemmon MA, Engelman DM, Brunger AT. The glycophorin A transmembrane domain dimer: Sequence specific propensity for a right handed supercoil of helices. Biochem. 1992; 31:12726–12733. [PubMed: 1463744]

44. Meyers GA, Orlow SJ, Munro IR, Przylepa KA, Jabs EW. Fibroblast-growth-factor-receptor-3 (FGFR3) transmembrane mutation in crouzon-syndrome with acanthosis nigricans. Nature Genetics. 1995; 11:462–464. [PubMed: 7493034]

45. Martinez-Frias ML, de Frutos CA, Bermejo E, Nieto MA. Review of the recently defined molecular mechanisms underlying thanatophoric dysplasia and their potential therapeutic implications for achondroplasia. Amer J Med Genet A. 2010; 152A:245–255. [PubMed: 20034074]

46. Peng WC, Lin X, Torres J. The strong dimerization of the transmembrane domain of the fibroblast growth factor receptor (FGFR) is modulated by C-terminal juxtamembrane residues. Protein Science. 2009; 18:450–459. [PubMed: 19165726]

47. You M, Spangler J, Li E, Han X, Ghosh P, Hristova K. Effect of pathogenic cysteine mutations on FGFR3 transmembrane domain dimerization in detergents and lipid bilayers. Biochem. 2007; 46:11039–11046. [PubMed: 17845056]

48. Moriki T, Maruyama H, Maruyama IN. Activation of preformed EGF receptor dimers by ligand-induced rotation of the transmembrane domain. J Mol Biol. 2001; 311:1011–1026. [PubMed: 11531336]

49. Beevers AJ, Damianoglou A, Oates J, Rodger A, Dixon AM. Sequence-dependent oligomerization of the Neu transmembrane domain suggests inhibition of "conformational switching" by an oncogenic mutant. Biochem. 2010; 49:2811–2820. [PubMed: 20180588]

50. Killian JA, von Heijne G. How proteins adapt to a membrane-water interface. Trends Biochem Sci. 2000; 25:429–434. [PubMed: 10973056]

51. Kim C, Schmidt T, Cho EG, Ye F, Ulmer TS, Ginsberg MH. Basic amino-acid side chains regulate transmembrane integrin signalling. Nature. 2012; 481:209–213.

52. Ozdirekcan S, Etchebest C, Killian JA, Fuchs PFJ. On the orientation of a designed transmembrane peptide: Toward the right tilt angle? J Amer Chem Soc. 2007; 129:15174–15181. [PubMed: 18001020]

53. Botelho AV, Huber T, Sakmar TP, Brown MF. Curvature and hydrophobic forces drive oligomerization and modulate activity of rhodopsin in membranes. Biophysical Journal. 2006; 91:4464–4477. [PubMed: 17012328]

54. Li PC, Miyashita N, Im W, Ishido S, Sugita Y. Multidimensional umbrella sampling and replica-exchange molecular dynamics simulations for structure prediction of transmembrane helix dimers. J Comp Chem online. 2013; doi: 10.1002/jcc.23494

55. Tang J, Yin H, Qiu JD, Tucker MJ, DeGrado WF, Gai F. Using two fluorescent probes to dissect the binding, insertion, and dimerization kinetics of a model membrane peptide. J Amer Chem Soc. 2009; 131:3816–+. [PubMed: 19256494]

56. Curnow P, Booth PJ. Combined kinetic and thermodynamic analysis of alpha-helical membrane protein unfolding. Proc Natl Acad Sci USA. 2007; 104:18970–18975. [PubMed: 18025476]

57. Limongelli V, Bonomi M, Parrinello M. Funnel metadynamics as accurate binding free-energy method. Proc Natl Acad Sci USA. 2013; 110:6358–6363. [PubMed: 23553839]

58. Koldsö H, Sansom MSP. Local lipid reorganization by a transmembrane protein domain. J Phys Chem Lett. 2012; 3:3498–3502. [PubMed: 26290979]

59. Monsonego-Ornan E, Adar R, Feferman T, Segev O, Yayon A. The transmembrane mutation G380R in fibroblast growth factor receptor 3 uncouples ligand-mediated receptor activation from down-regulation. Mol Cell Biol. 2000; 20:516–522. [PubMed: 10611230]

60. Cho JY, Guo CS, Torello M, Lunstrum GP, Iwata T, Deng CX, Horton WA. Defective lysosomal targeting of activated fibroblast growth factor receptor 3 in achondroplasia. Proc Natl Acad Sci USA. 2004; 101:609–614. [PubMed: 14699054]
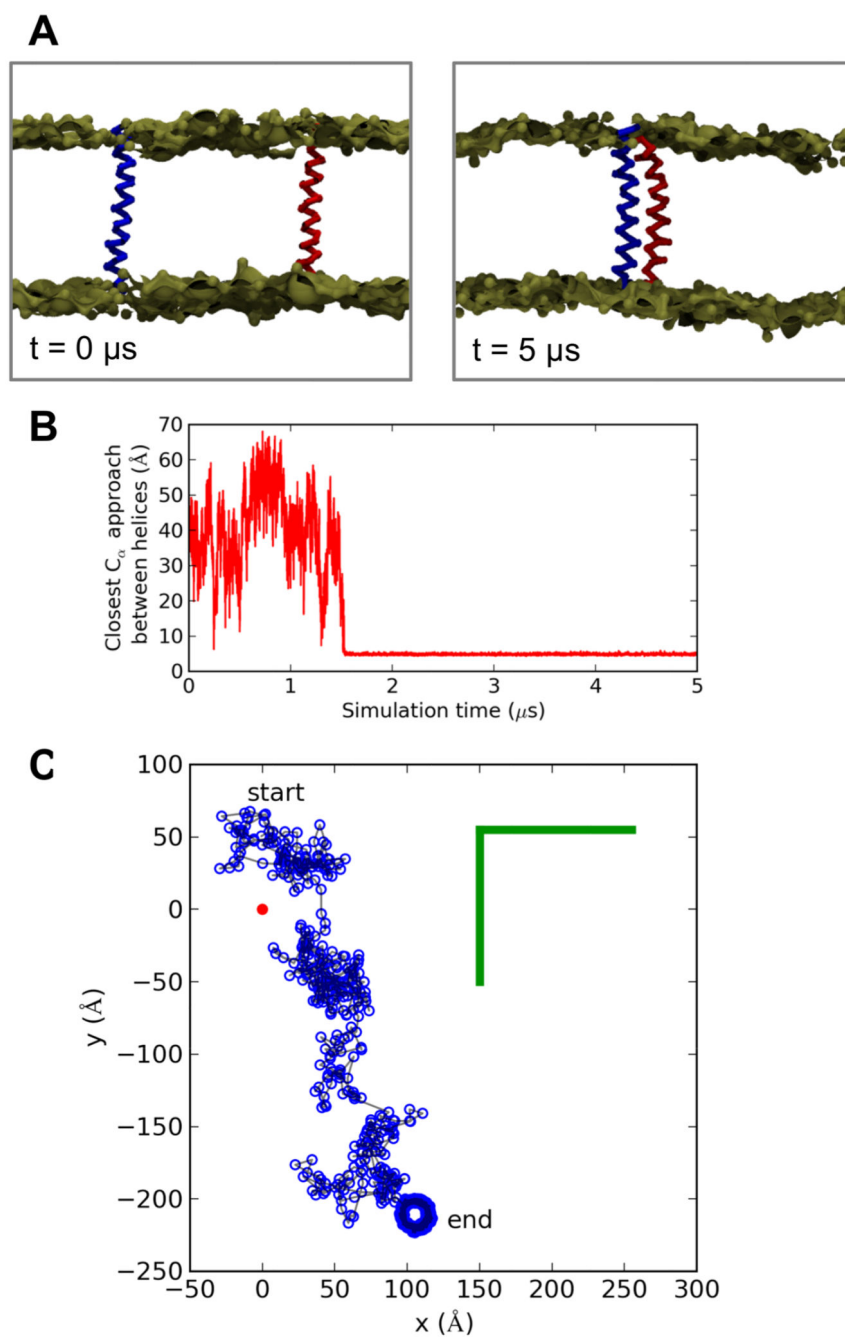
Figure 1.
A: Initial (t = 0) and final (t = 5 μs) configurations of a WT FGFR3 CG simulation showing the two helices as C_α traces in red and blue with the bronze spheres corresponding to a surface representation of the phosphate particles of the lipids. Other lipid and solvent particles are omitted for clarity. **B:** The C_α helix-helix approach is shown as a function of time for the same WT FGFR3 CG simulation as in **A**. **C:** The relative motion of the centroid of helix 2 (blue) in the reference frame of the centroid of helix 1 (red) is shown for the same FGFR3 WT CG simulation as in **A,B**. Coordinates of helix 2 are plotted every 10th frame of

the simulation (i.e. every 4 ns) in the *xy* plane (which is approximately equivalent to the bilayer plane). The approximate size of the simulation box in the *xy* plane is shown in green.
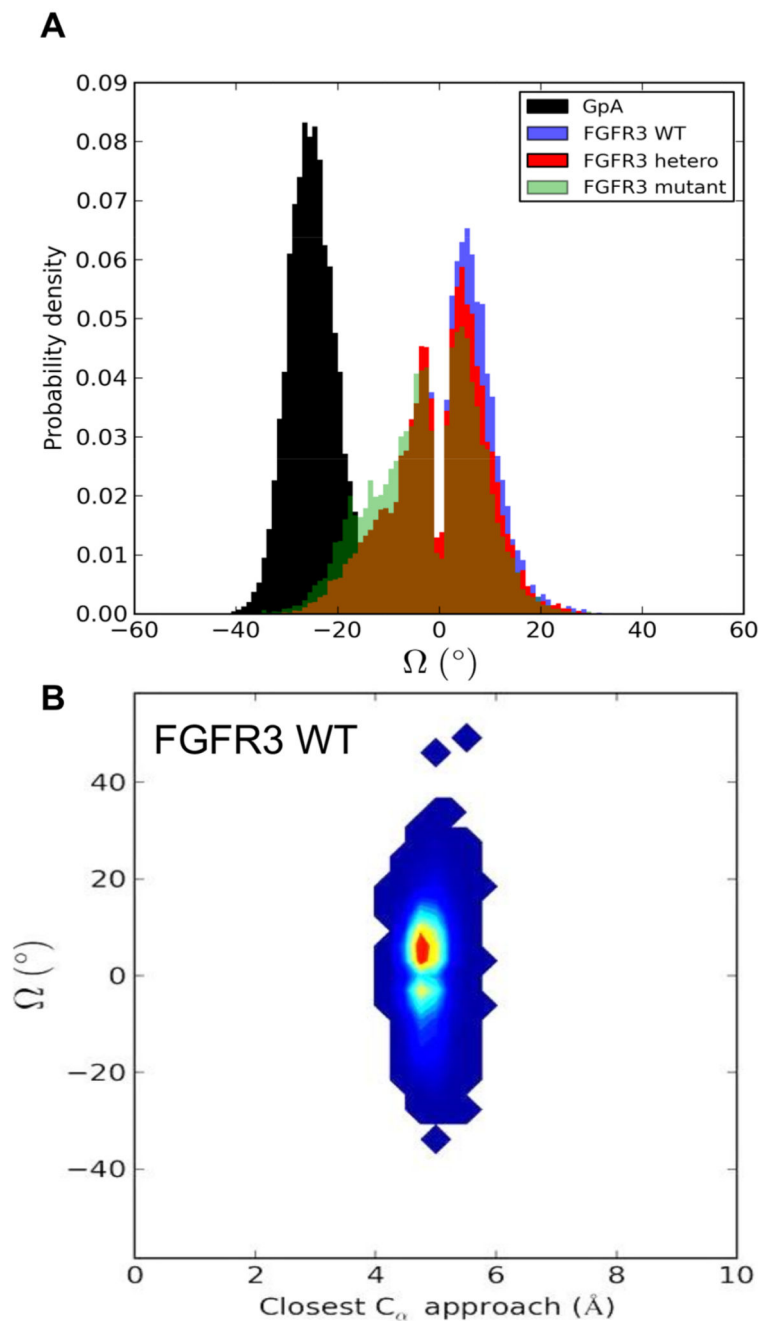
Figure 2.
A: Helix crossing angle (Ω) distributions for the merged (see Table 1) FGFR3 WT (blue), FGFR3 WT/G380R heterodimer (red), FGFR3 G380R homodimer (green), and GpA (control, black) simulations. Every 25th frame (i.e. every 10 ns) of the constituent trajectories was parsed and included in the histograms only if the helices were dimerized (10 Å interhelix centroid distance cutoff). **B:** The helix crossing angle (Ω) vs. C_α helix-helix approach distribution is shown for the FGFR3 WT simulations, using an ascending blue to yellow to red heatmap.
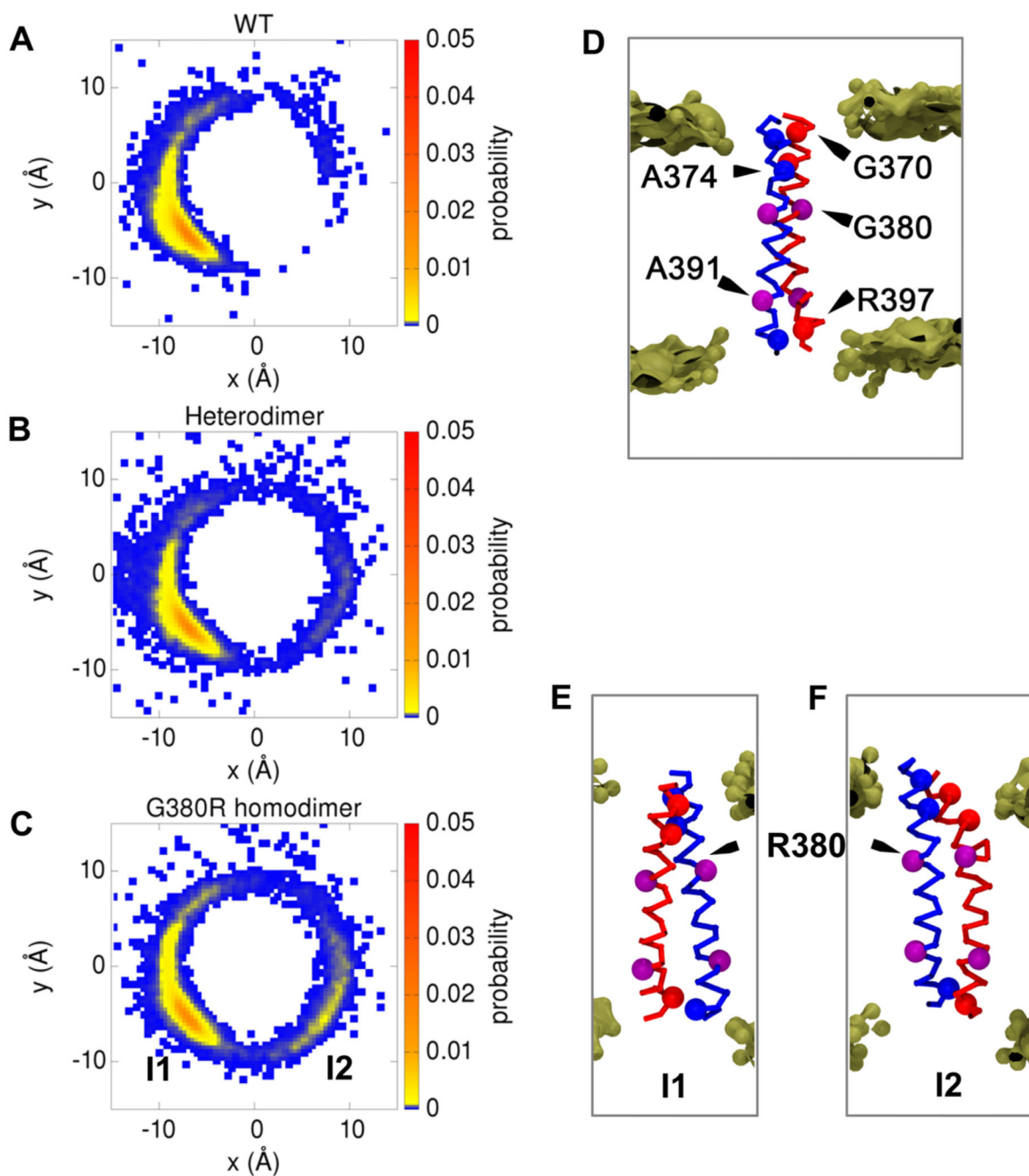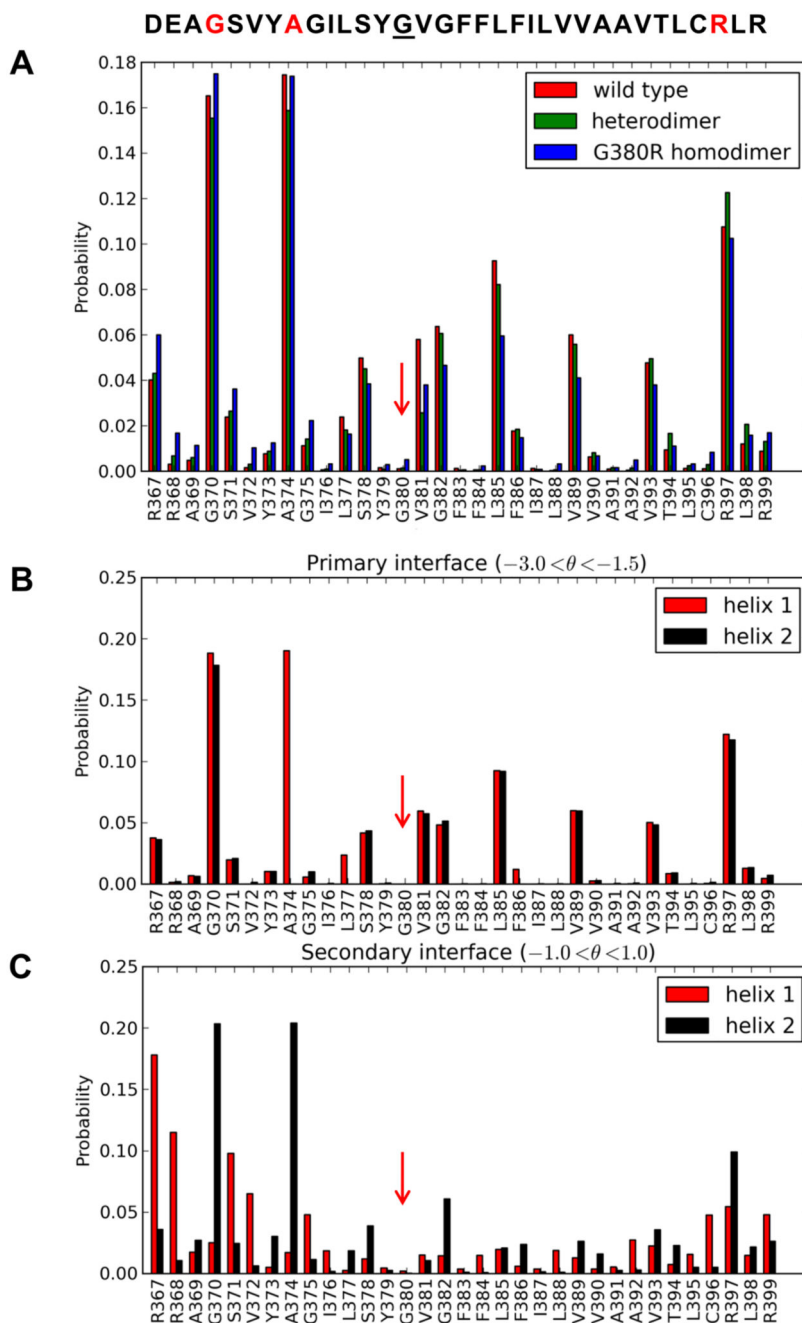
Figure 3.
A-C: The positional probability of the geometric center of helix 2 relative to helix 1 in the *xy* plane is shown as a non-linear (ascending: blue to yellow to red) heat map for the FGFR3 WT (**A**), FGFR3 WT/G380R heterodimer (**B**), and FGFR3 G380R homodimer (**C**) simulations. To generate these maps each frame of a simulation is aligned by RMSD fitting of helix 1 onto the configuration of that helix in the first frame of the FGFR3 wildtype simulations. **D:** Representative structure of the WT helix dimer, corresponding to the maximum probability in **A**. The C_α of key residues forming the predominant interfacial

contacts (G370, A374, and R397; see main text and Figure 4) are shown as red and blue spheres, whilst the disease-related residues G/R380 and A391 are shown in purple. The bilayer phosphate particles are shown as bronze spheres (surface representation). **E:** Representative structures of the G380R mutant homodimer, corresponding to the two peaks in probability I1 (**E**) and I2 (**F**) in **C**.

Figure 4.
A: Normalized frequency of occurrence for a residue to be in the five closest contacts between helices. A dimer is defined as when the interhelix (C_α particle) separation is within 7 Å over all the CG simulations of an ensemble. Results are merged for both helices 1 and 2 of the wild-type (red), heterodimer (green) and G380R mutant homodimer (blue) simulations. **B:** Normalized frequency of occurrence for a residue in the five closest contacts between helices (defined as when the interhelix (C_α particle) separation is within 6 Å) for the primary (I1 in Fig. 3) interface showing helix 1 and 2 in red and black respectively. **C:**

Normalized frequency of occurrence for a residue in the five closest contacts between helices in the secondary (I2 in Fig. 3) interface. The vertical red arrows indicate residue G380.
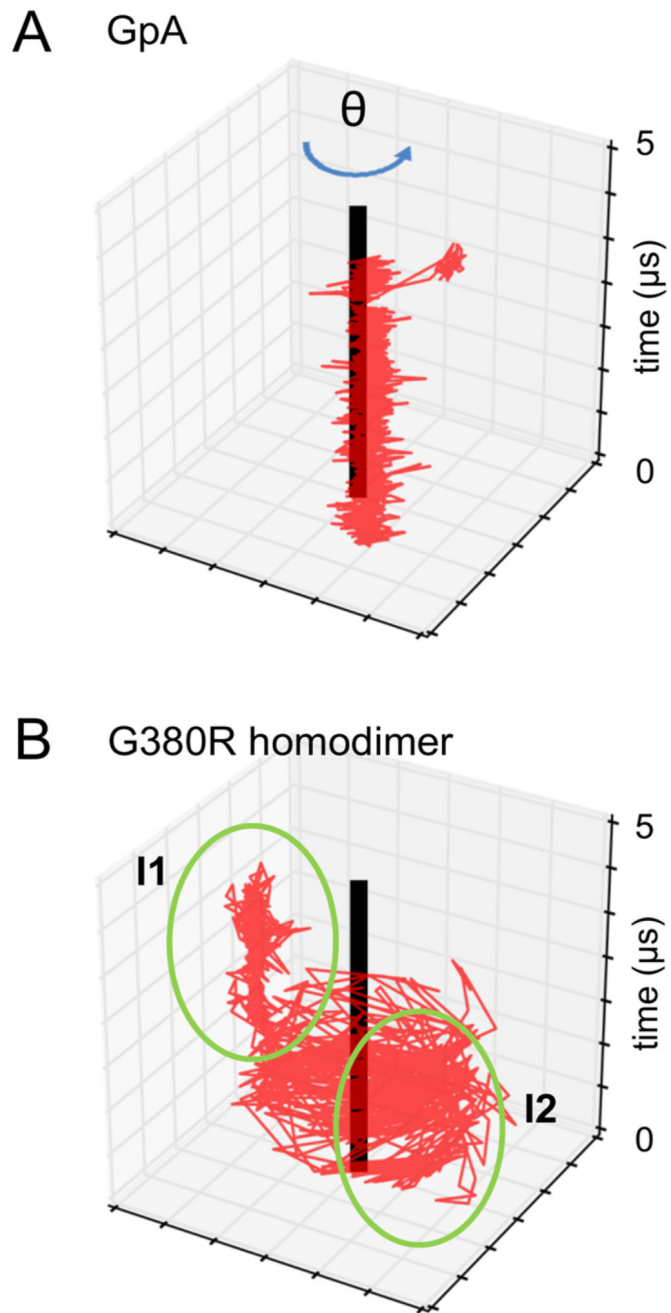
Figure 5.
Position of the geometric center of helix 2 (red) relative to helix 1 (black) in the xy plane as a function of time (the vertical axis). This is shown for representative simulations from the **A** GpA and **B** FGFR3 G380R mutant homodimer ensembles. For the G380R simulation the green rings indicate the primary (I1) and secondary (I2) interfaces (see Fig. 3 and text).
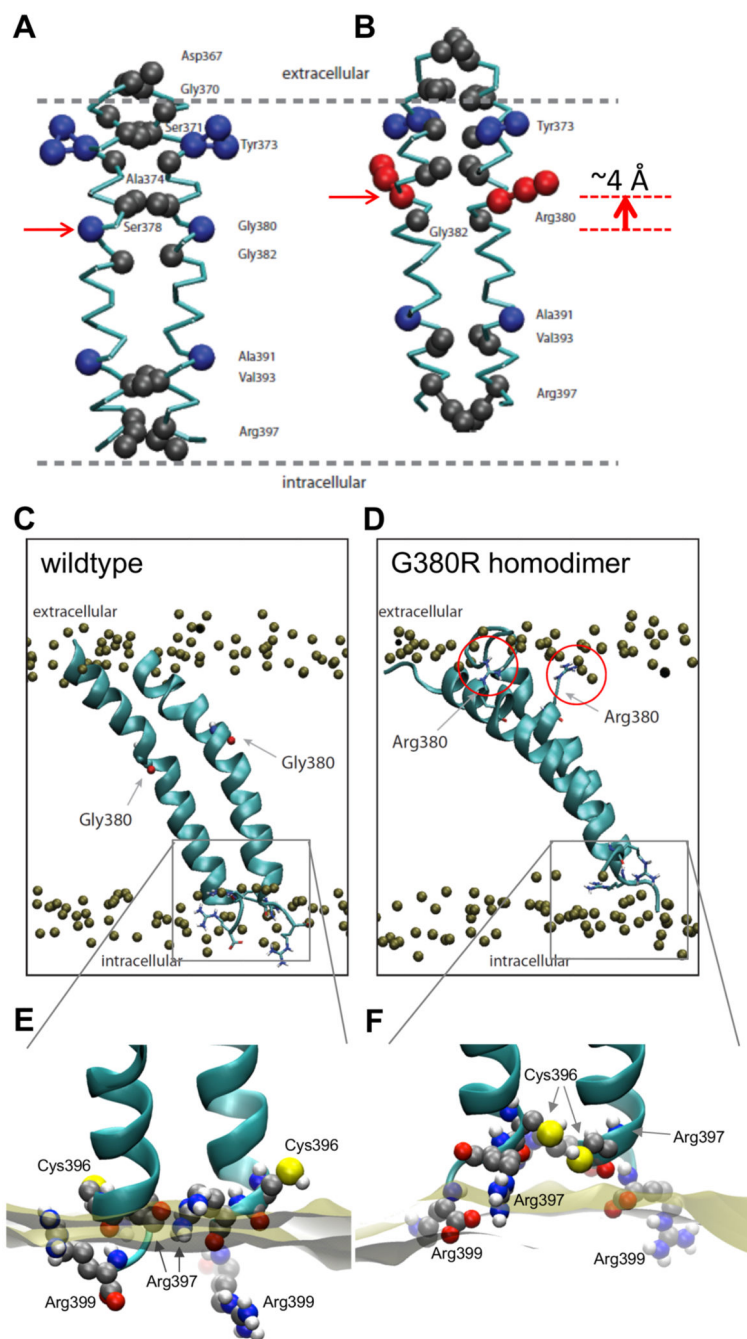
Figure 6.
A, B: Representative models corresponding to the primary helix/helix interface (I1 in Fig. 3) for the wild-type (**A**) and G380R homodimer (**B**) CG simulations. The Cα backbone is coloured in cyan. The closest contact residues are shown as grey spheres and disease-related residues (Y373, G380 and A391) as blue spheres. The two dashed lines indicate the approximate position of the phosphate particles of the CG lipid bilayer. The horizontal arrows indicate the residue at position 380, G in the wild-type and R (red) in the mutant.

C,D: Atomistic simulations of the wild-type (**C**) and G380R mutant (**D**) homodimer helix dimers starting from the structures shown in **A** and **B** respectively. The final frames of the 100 ns AT-MD simulations are shown. The phosphorus atoms of the lipids are shown as bronze spheres. In **C** the G380 atoms are shown; in **D** the R380 sidechains forming 'snorkelling' interactions with lipid phosphates are shown in bond format and highlighted with red circles.

E,F: Detailed view of protein-lipid interactions at the inner membrane leaflet. The atoms of C396, R397 and R399 are shown as spheres, coloured according to atom type. The bronze surface represents the position of the membrane phosphate particles. In the WT simulation (**E**) The $C_{396}RLR_{399}$ residues are located around the phosphate periphery whereas the G380R mutation (**F**) pulls those residues towards the membrane core, resulting in a rotation of the C-terminal TMD section.

Table 1

Summary of Simulations

TMDs	Force-field	Duration
FGFR3		
WT	CG, modified MARTINI[†]	10 x 5 μs[*] and 20 x 1 μs[**]
WT/G380R	CG, modified MARTINI	10 x 5 μs[*]
G380R	CG, modified MARTINI	10 x 5 μs[*] and 20 x 1 μs[**]
WT	AT[‡]	0.1 μs
G380R	AT	2 x 0.1 μs
GpA (control)		
WT	CG, modified MARTINI	5 x 5 μs

[*] These simulations are the basis of the main analysis shown in Figures 1 to 4. The sequence used was as previously employed in (10) with the G380 residue in bold: RRAGSVYAGILSY**G**[380]VGFFLFILVVAAVTLCRLR.

[**] These simulations were used to generate representative structures from which to initiate the atomistic simulations. The sequence employed was: DEAGSVYAGILSY**G**[380]VGFFLFILVVAAVTLCRLR.

[†]The modified MARTINI forcefield is as described in (25).

[‡]Atomistic simulations were run using the GROMOS forcefield (37) gromos43a1.